Light-triggered simultaneous release of reactive oxygen species and thymol from mesoporous organosilica particles with potential application in deep tissue

Hannah Bronner[1], Katharina Doll-Nikutta[2,3], Muhammad Imran Rahim[2,3], Sören Donath[3,4], Nina Ehlert[4], Yaşar Krysiak[1], Alexander Heisterkamp [3, 4], Meike Stiesch[2,3], Stefan Kalies[3,4]*, Sebastian Polarz[1]*

[1]Institute of Inorganic Chemistry, Leibniz University Hannover, Callinstraße 3-9, 30167 Hannover

[2]Department of Prosthetic Dentistry and Biomedical Materials Science, Hannover Medical School, Carl-Neuberg-Str. 1, 30625 Hannover, Germany

[3]Lower Saxony Centre for Biomedical Engineering, Implant Research and Development (NIFE), Stadtfelddamm 34, 30625 Hannover, Germany

[4]Institute of Quantum Optics, Leibniz University Hannover, Welfengarten 1, 30167 Hannover, Germany

Corresponding author's email: Stefan Kalies: Kalies@iqo.uni-hannover.de, Sebastian Polarz: Sebastian.polarz@aca.uni-hannover.de

Keywords: alternative antibiotics, triggered drug release, antibacterial photodynamic therapy, two-photon irradiation, mesoporous organosilica nanoparticles.

Abstract

Antibiotic resistance in bacterial pathogens is a global health problem requiring enormous research into alternative, easily accessible antibacterial substances and treatments to replace antibiotics. Components of essential oils (EOs) that possess broad-spectrum antibacterial properties are promising candidates. However, due to their high volatility and low solubility, their administration remains difficult. A promising method is to load materials with the active component and design a triggered release system to avoid rapid exhaustion of the carried material. If such a drug-release system would additionally exhibit antibacterial properties itself, it could significantly advance combatting bacterial infections. Therefore, in the present study, we combine the light-triggered and simultaneous release of the antimicrobial substance thymol with antibacterial photodynamic therapy (aPDT) within one nanoparticle. The irradiation of an

immobilized photosensitizer produces reactive oxygen species (ROS) that oxidatively cleave a linker and ultimately releases thymol detected by GC-MS. Antibacterial properties towards *Staphylococcus aureus* biofilm formation were verified by ATP-based viability assay. To improve the application for deep tissue delivery, we also take into account the low transmittance of visible light. A highly developed trifunctional material enables 2-photon excitation via Förster resonance energy transfer (FRET) and thus shifts the wavelength into the biological window. The release of the third functionality can be monitored *in situ* by fluorescence microscopy. This model system lays the foundation for future antibacterial materials.

1. Introduction

A recent study estimates that in 2019, 4.95 million deaths worldwide were associated with bacterial antimicrobial resistance (AMR).[1] AMR is mainly caused by the incorrect and excessive use of antibiotics. The development of new types of antibiotics is extremely cost-intensive and time-consuming.[2] Resistance is detected on average two to three years after the market launch of most new active substances.[2] That is why there is an urgent need to find alternative therapy methods against bacterial infections and prevent them. The last decade has seen substantial advantages in developing highly advanced drug-delivery systems (DDS).[3–5] Because of the given arguments, materials that release antibiotics are under debate. Therefore, alternative compounds with similar biocidal activity were searched and how those species can be delivered by specialized materials.

The so-called reactive oxygen species (ROS) such as superoxide ($O_2^{\bullet-}$), singlet oxygen ($^1O_2$), hydroxyl radical ($HO^{\bullet}$), and hydrogen peroxide (H_2O_2) show excellent properties against bacteria which can hardly protect themselves because of the low specificity and high chemical power of the ROS species. The use of ROS species in a medical context has led to the emergence of the antibacterial photodynamic therapy (aPDT) field.[6] The ROS species are formed by a photocatalytic process. The photogenerated charge carriers in semiconductors or chromophores react with oxygen or water molecules. Thus, another advantage of aPDT is that it is sustainable. It can be activated by irradiation with light. aPDT-systems work great in *in-vitro* experiments because one can expose the materials to high doses of light in the UV or Vis spectral range. For instance, we have developed mesoporous organosilica materials (MOPs) containing organic dyes capable of ROS production.[7] However, the absorption features of the dye required high energy of light ($\lambda < 500$ nm) for activation. The latter is a principle problem.[8] The photoreduction of oxygen requires excited electrons with higher energy than the acceptor

orbitals of the substrate, which, in turn, means that the energy of red light is insufficient. Skin, or biological tissue generally, is not transparent for UV/Vis light. ROS-producing aPDT systems working with near-infrared (NIR) light are highly desired.[9] There are several possibilities to push the absorption wavelength of a photoactive compound into this window by energy-upconverting nanoparticles and complex NIR-dyes.[10] A more straightforward strategy is the use of two-photon excitation, which enables confining effects to the focal volume and reaches high penetration with NIR wavelengths. As conventional photosensitizers are poor two-photon absorbers, nanoparticles have been developed that combine a dual system where a strong two-photon absorber transfers its energy to an effective photosensitizer via Förster resonance energy transfer (FRET).[11,12] A promising candidate for the two-photon absorber is Acridine Orange[13–15], which has an emission spectrum with a high overlap to the absorption spectrum of the already applied photosensitizer Rose Bengal.

Another alternative compound class to prevent colonization and biofilm formation is essential oils (EOs), which have attracted attention as plants use them to defend against bacterial, viral, and fungal infections.[16–18] Biofilms are bacterial agglomerates that are surrounded by a self-produced matrix from extracellular polymers and an additional altered metabolic phenotype. These characteristics increase the resistance of bacteria to antibiotics about 1000-fold.[19] Biofilm formation is initially mechanically induced by surface contact, leading to adherence and microcolony formation.[20] A synchronous bacterial behavior and pathogenicity development are then regulated by an intercellular concentration-dependent transcription factor system called quorum sensing (QS).[21] One integral part of EOs with an anti-microbial activity is thymol, a natural monoterpenoid characterized by its strong bactericidal, fungal, and antiparasitic properties with relatively low toxicity for humans. Its antimicrobial action is attributed to its disruption of bacterial cell membranes.[22] Thymol has been identified to reduce bacteria biofilm formation in subinhibitory concentrations.[23] The anti-QS properties of thymol and essential oils containing thymol have already been described against various pathogens.[24–28] Because thymol is only slightly soluble in water at neutral pH and is volatile, developing a heterogeneous support for drug delivery is desirable.[29,30] Compounds like cellulose acetate,[31] zein[32], or lignosulfonate[33] can be used, but they feature a problem many drug-delivery systems have: The release starts instantaneous and is steady, which could lead to undesirable side effects and rapid material depletion. Stimuli-responsive, respectively smart materials represent the next generation of DDS, for instance, discussed by Kesharwani et al. in 2024.[34] So far, no triggered release system for thymol-loaded carriers has been described.

Many studies show that the viability of the bacteria is reduced when the drug-delivery system is presented. Often, a minor fraction of the bacteria survive. This does not have to be a problem if the immune system can fight the damped infection on its own. However, it can be that the bacteria surviving the initial attack recover, and the biofilm continues growing. Therefore, DDS capable of killing all bacteria are preferred. Because one has learned that the latter goal is difficult to achieve using only one antibacterial compound, the 'synergistic killing' concept has been established. For instance, synergistic strategies have been developed that combine aPDT with antibiotics, antimicrobial agents, photothermal therapy, or nitric oxide (NO) therapy.[35] Here, we want to introduce a new and synergistic antibacterial DDS system. The system should not only produce ROS species, it should be activable by NIR light, and thymol release itself is triggered by the presence of those ROS species. The latter will be realized by using an oxidatively cleavable linker. Such linkers, like vinyl ether, vinyl disulfides, or amino acrylates, have been studied as anti-cancer drug release systems but barely in antibacterial applications.[36] Li *et al.* have developed gated mesoporous silica nanoparticles loaded with the antibiotic vancomycin, which is released upon interaction with ROS in the microenvironment of bacteria.[37] However, the release of an antimicrobial small molecule by the cascade reaction of the light-triggered excitation of a photosensitizer, which generates ROS that ultimately cleaves an oxidatively cleavable linker and releases the molecule, has not been described so far. The material architecture and the overall concept are shown in **Scheme 1**. The surfaces of organosilica nanoparticles are equipped with three different functional groups using the Michaelsen thiol-ene click chemistry. The acridine orange (AO) derivate is responsible for the upconversion of NIR light via two-photon processes and transfer to the Rose Bengal (RB) derivate. RB then generates ROS species. The ROS species do not only exhibit antibacterial action, but synergistically they cleave the linker of the surface attached thymol molecule. We will study the ROS production and thymol release from MOPs with a special emphasis on the system's long-term stability in a technical and biological environment. We will then explore the potential of the nanoparticles to release a drug under two-photon excitation and, thus, ensure their application in deeper tissues.

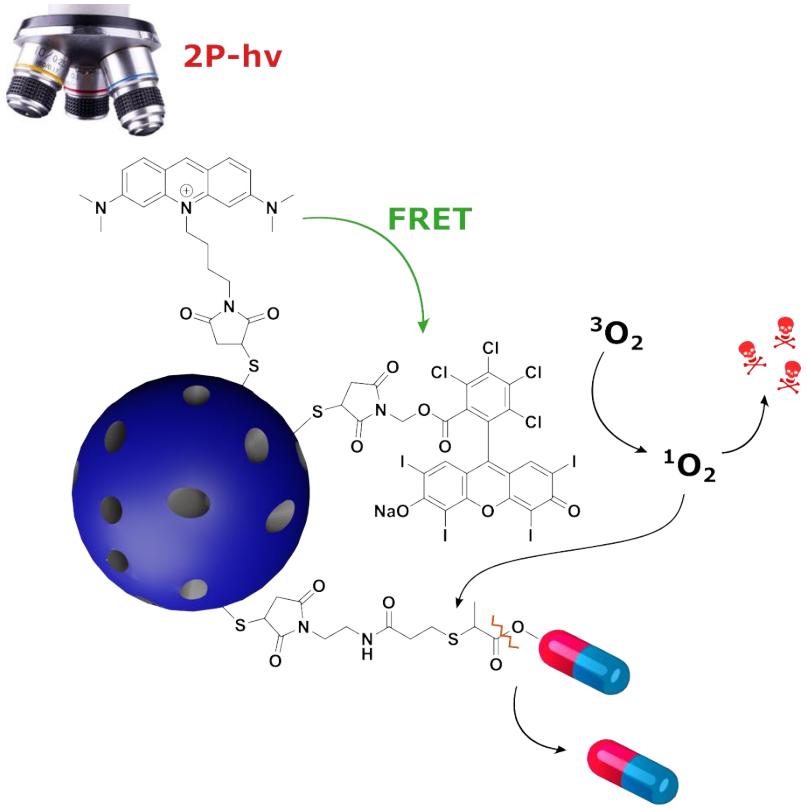

Scheme 1: Schematic representation of functionalized MOPs for the ROS-triggered release of a drug using 2-PE excitation for deep tissue application. Irradiation starts the cascade reactions: (1) excitation of Acridine Orange, (2) FRET transfer of the energy to Rose Bengal, which transfers its energy to excite triplet oxygen to singlet oxygen (3) and finally the ROS species oxidizes and cleaves the linker and releases the drug (4).

2. Results and Discussion

2.1. Maleimide Modification of Functional Molecules.

For covalent anchoring of the mentioned organic groups on the surfaces of phenylthiol-containing MOPs developed in our group in the past,[7,38] the compounds have to be modified by a maleimide functionality. The photosensitizer Rose Bengal was reacted with *N*-chloromethyl maleimide. The reaction scheme is depicted in the Supporting Information **Scheme S2,** and analytical data are given in **Figures S51- 56**. The synthesis protocol leading to the Thymol derivate containing the ROS-cleavable and the clickable functionalities, named as ROS-Thymol, is described in detail in the Supporting Information; see **Scheme S3 and S4**. Characterization data for all intermediates and products is depicted in **Figures S57- 73**. The preparation of a maleimide modified acridine orange compound has been described previously.[9]

2.2. Surface Functionalization of Mesoporous Organosilica Nanoparticles.

MOPs containing phenylthiol were reproduced from ref.[9] The post-functionalization of MOPs was achieved by base-catalyzed Thiol-Michael addition click reaction of the thiol groups on the pore walls. We describe the synthesis and properties of mono-functional particles first and then increase the number of functional groups that are attached to the surfaces successively.

A representative scanning electron microscopy (SEM) image of the resulting particles is given in **Fig. 1a**. The detailed experimental procedure can be found in the supplementary information and additional data for characterization of the different MOPs; **Figures S1- S15**.

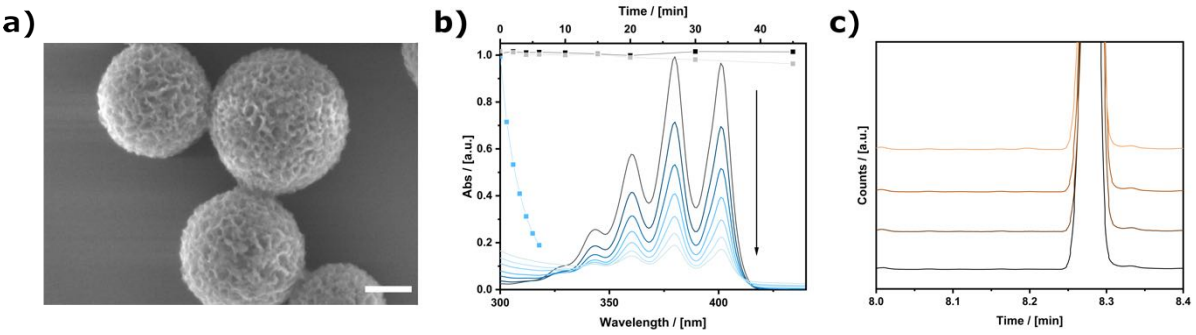

Figure 1. a) Exemplary SEM image of MOPs-ROS-Thymol (scale bar = 100 nm). b) ABDA assay of MOPs-RB under irradiation with green LED confirming ROS-production (black: t = 0 min to light blue: t = 6 min, a measurement was taken every minute). Arrow indicating the decomposition of ABDA. Time-dependent decomposition of ABDA under different conditions: irradiation with green LED (blue dots), kept in the dark (black dots), and kept at daylight (grey dots). c) GC-MS chromatogramm of MOPs-ROS-Thymol that were kept in the dark (black: t = 0 min, dark brown: t = 20 min, light brown: t = 4 h, orange: t = 24 h). Intensity is normalized to internal standard.

For MOPs-RB, the amount of immobilized ROS producer could be determined to 96.1 µg per mg particles (see **Figure S6- S7**). The ROS production was examined by monitoring the decomposition of ABDA (9,10-anthracenediyl-bis(methylene)dimalonic acid) with UV-Vis measurements of the particle-free supernatant. ABDA is specific to singlet oxygen production.[39] **Figure 1b** depicts the result of the ABDA assay and confirms that MOPs-RB nanoparticles could produce ROS under irradiation at 530 nm. Importantly, there was no ROS production when the particles were kept dark. Furthermore, the exposure to room lighting did not result in a significant ROS release (see **Figure 1b**, black and grey lines). These important findings ensure that ROS production can be exclusively triggered by light of a specific

wavelength and that the particles can be handled without leakage. Therefore, the first component of the bifunctional material was established successfully.

Next, MOPs-ROS-Thymol was prepared. Characterization data is given in the Supporting Information (see **Figure S13 and S14**). The amount of immobilized thymol was quantified as 68.6 µg per mg particles. Sharma *et al.* proposed a mechanism for the oxidative cleavage of the used linker and the subsequent release of the active drug.[40] After oxidation of the thioether to its corresponding sulfone or sulfoxide, these relatively hydrophilic intermediates promote the hydrolysis of the phenolic ester. Hence, there is a fine line between the ideal molecules to be released, as the aromatic ester must be cleavable after oxidation but still be stable towards aqueous hydrolyzation.[41] To investigate the stability of the phenolic ester under a non-oxidative environment, MOPs-ROS-Thymol were suspended in PBS, kept in the dark and the supernatant was analyzed for released thymol. The resulting GC-MS measurement is depicted in **Figure 1c**. The signal of the released thymol would have been expected at a retention time of t = 8.19 min. However, even after an incubation time of 24 hours there was no significant release of thymol visible. UV-Vis spectra of the supernatant confirm the data (see **Figure S15**). For application, it is also desirable that the samples can be stored before use without losing their loaded drug. To test the long-term stability, MOPs-ROS-Thymol were stored in the fridge for 35 days and tested again for unwanted leakage of thymol. UV-Vis measurements of the supernatant confirm its long-term storage stability as there was still no signal for thymol detectable (see **Figure S15**). These conclusive results showed that the necessary criteria for long-term stability were fulfilled.

Finally, the bifunctional material containing the Rose Bengal photosensitizer and the ROS cleavable thymol (MOPs-RB-ROS-Thymol; **Fig. 2a**) were synthesized. The characterization of the binary materials can be found in **Figure S16- S20**. The relative amount of RB : ROS-Thymol can be controlled by the ratio of the molecules used in the reaction solution m : n; see **Table S10**. The samples are named MOPs-RB^{m}-ROS-Thymol^{n}. As expected, also for the bifunctional MOPs there is no leakage of Thymol (see **Figure S20**). The ROS production of binary MOPs-RB-ROS-Thymol was investigated using the ABDA assay under the same experimental conditions (see **Fig. 2b** and **Fig. S22**). As expected, the rate of ROS production scales to the amount of photosensitizer present on the surfaces.

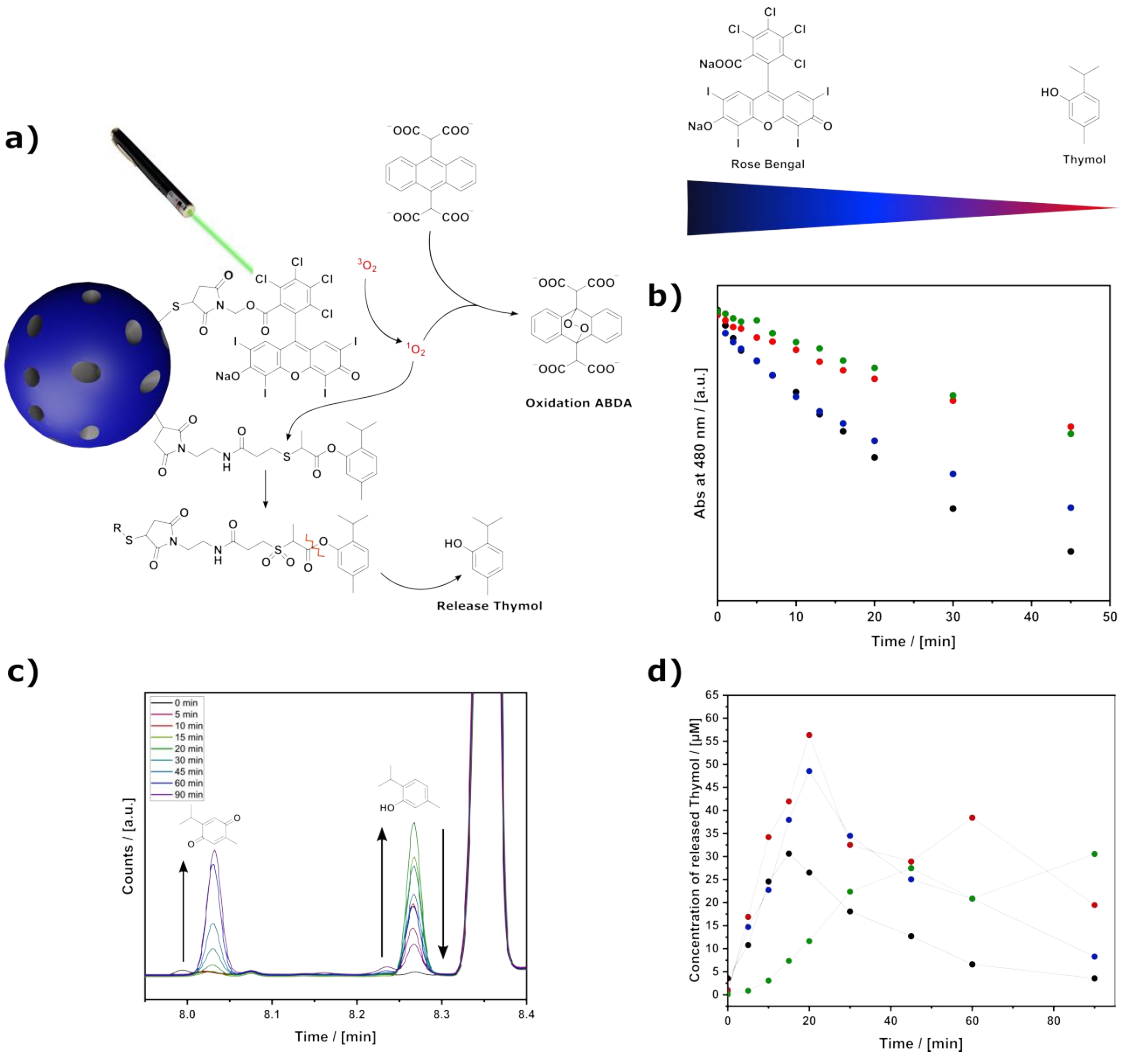

Figure 2. (a) Schematic mechanism of ROS detection via ABDA assay and oxidation and release of thymol. (b) ROS detection via ABDA assay; black: MOPs-RB[1]-ROS-Thymol[2], blue: MOPs-RB[1]-ROS-Thymol[10], red: MOPs-RB[1]-ROS-Thymol[20], green: combined MOPs-RB and MOPs-ROS-Thymol with ratio 1 to 10. and thymol release of MOPs-RB-ROS-Thymol (c and d) with (c) exemplary GC-MS measurements of MOPs-RB[1]-ROS[10]-Thymol, arrows mark increasing and decreasing released amount of thymol and increasing oxidation of thymol and c) released concentration of thymol of different MOPs-RB-ROS-Thymol samples

To analyze the release of thymol, aliquots of the suspension were taken after irradiation, the particles were filtered off, and the clear supernatant was analyzed by GC-MS. **Figure 2c** depicts an exemplary GC-MS measurement (the rest can be found in **Figure S23** and **S24**). Irradiation led to the formation of new peaks at t = 8.02 min and t = 8.26 min (the signal at t = 8.35 min belongs to the internal standard). The peak at t = 8.26 min could be assigned to released thymol (**Figure 2c**). Interestingly, the second peak at t = 8.02 min could be attributed to thymoquinone (see **Figure 2c**) which is the oxidized form of thymol. Oxidation to thymoquinone is not a

disadvantage for the material, as thymoquinone has anti-cancer[42] and antibacterial properties and inhibits biofilm formation and virulence.[43–45] Its higher selectivity towards bacteria than towards human cells has also been demonstrated.[46] Lu *et al.* even intentionally oxidized thymol to thymoquinone and initialized the ROS production by thymoquinone.[47] Therefore, the specific antibacterial properties of thymoquinone produced by the bifunctional particles would be interesting to analyze in a further study. Comparing the time-dependent thymol release of binary MOPs-RB-ROS-Thymol led to the conclusion that the more Mal-ROS-Thymol is immobilized on the particle, the higher is the released amount of thymol (see **Figure 2d**). The highest release of thymol could be reached with 56.4 µM MOPs-RB^{1}-ROS-Thymol^{20} (a used ratio of Mal-RB: Mal-ROS-Thymol of 1: 20) after an irradiation time of only 20 minutes (see **Figure 2d, red dots**). After that time, the amount of free thymol decreased again due to the oxidation of free thymol to thymoquinone. Furthermore, the immobilization of both functions on one particle had a synergistic effect: when compared to the monofunctionalized particles, the bifunctionalization showed an earlier and more efficient release (see **Figure 2d**, green dots). By this, the functionalized MOPs allow for tuning the release properties and adjusting them specifically for any future application.

2.3. Antibacterial properties of MOPs-RB-ROS-Thymol

Initial experiments to test the antibacterial activity of MOPs-RB-ROS-Thymol were carried out with *Staphylococcus aureus*, a commensal skin bacterium highly associated with nosocomial infections. To initially test the biocidal effect of pure thymol, it was added to *Staphylococcus aureus* during biofilm formation in concentrations comparable to the particle's release characteristics. After an incubation time of 24 h, the bacterial metabolic activity was determined by ATP quantification.[48] This method was selected over the measurement of optical density or fluorescence-based metabolic activity assays to avoid falsification by the particle's high turbidity and strong dye uptake properties. **Figure 3a** shows that the viability of *S. aureus* continuously decreased with increasing thymol concentration, being statistically significantly lower from 62.5 µg/mL. This antibacterial effect could probably be attributed to the described quorum sensing inhibition of thymol, but might also include further mechanisms that need to be analyzed in the future.

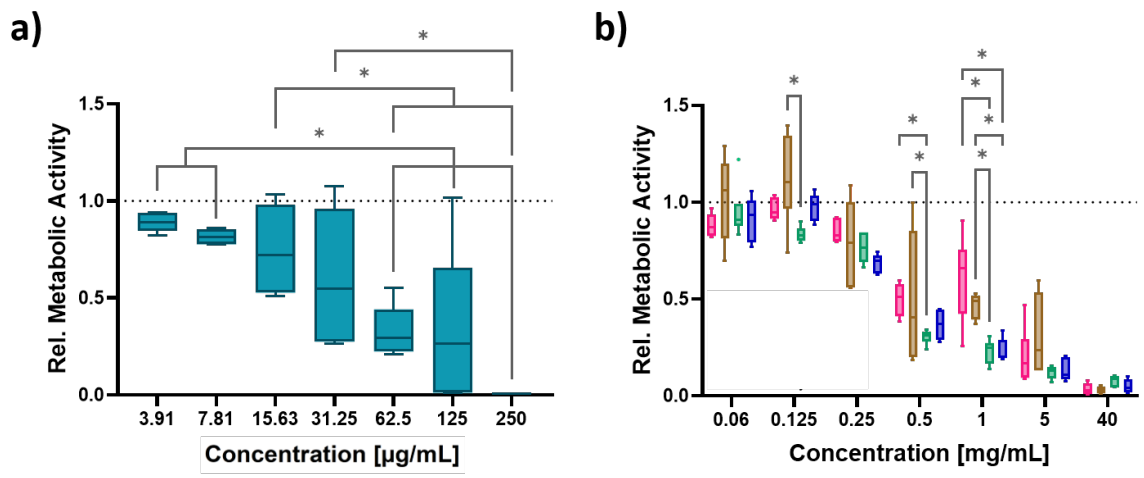

Figure 1: Antibacterial effect of dissolved thymol (a) and functionalized MOPs (b) against Staphylococcus aureus (pink: MOPs-RB not irradiated; brown: MOPs-RB irradiated for 20 min with 520 nm; green: MOPs-RB^{1}-ROS-Thymol^{20} not irradiated; blue: MOPs-RB^{1}-ROS-Thymol^{20} irradiated for 20 min with 520 nm).

To test the antibacterial properties of MOPs-RB^{1}-ROS-Thymol^{20}, different concentrations were dispersed in PBS buffer, incubated with bacteria during biofilm formation, and analyzed by ATP-quantification as described above. Particles that were only functionalized with Rose Bengal (and, thus, only produced ROS but not thymol when irradiated) were used as a control. As shown in **Figure 3b** increasing particle concentration led to a decrease of bacterial viability for all conditions. The decrease was statistically significant from concentrations of 0.25 mg/mL for irradiated particles and from concentrations of 0.5 mg/mL for non-irradiated particles. Furthermore, at medium concentrations, the metabolic activity of *S. aureus* that were treated with particles containing thymol was significantly lower than the ones without thymol. These results indicate two things (within the limitations of these initial antibacterial tests): 1) Even though irradiated and non-irradiated particles of similar functionalization and concentration do not show statistically significant differences per se, there seems to be a certain beneficial effect of UV-activated ROS production. Furthermore, additional thymol addition increases the antibacterial properties as expected by adding another antibacterial mechanism to the system.[24–28,49] 2) The modified particles also exhibit antibacterial properties beyond the expected light-triggered bifunctional mechanism. This could be either due to active functional groups and the bare particles or an alternative activation of the bifunctional mechanism. Recently, we could quantify ROS production by the used *S. aureus* strain itself.[50] It would be possible that the ROS produced by the bacterium itself are sufficient to release an effective amount of thymol. This would give the material a second activation system, without light, simply by the presence of bacteria. Taking these findings into account, we could consider the system as a two-way antibacterial release system. If ROS-producing bacteria are present thymol is released autonomously and the infection is treated. If this is not sufficient, or bacteria are

present which do not produce ROS, thymol release can be boosted externally by light exposure. Such a two-way release system would have enormous potential for biomedical applications and this hypothesis will be explored in detail in the future.

2.4 MOPs for 2-photon absorption and ROS production

Even though the previously described MOPs-RB-ROS-Thymol show promising antibacterial properties, their application is bound to superficial infections due to the limited depth of tissue penetration by light (considering no autonomous activation by the bacteria themselves). For this purpose, we additionally aimed to improve the system in terms of ROS production under irradiation, which penetrates deep into the tissue. Therefore, we used the strategy of the simultaneous absorption of two photons, which also ensures highly localized excitation.

To realize this, a binary system of an absorber of 2-photon excitation (2-PE) in combination with the previous Rose Bengal photosensitizer was used. As described in **Scheme 1**, the material should work the following way: the dye Acridine Orange can absorb the 2-PE irradiation and transfer it via FRET to the photosensitizer Rose Bengal, which then produces ROS. A high FRET efficiency is dependent on two aspects: a high overlap of donor emission and acceptor absorption spectrum as well as a close distance between both molecules. As shown in **Figure 5a**, the optical properties of both dyes fulfill these requirements and immobilizing Acridine Orange and Rose Bengal onto a solid substrate provides the close distance. To analyze the optical properties of the binary material and draw correlations to the resulting release, different ratios of both dyes were immobilized on MOPs and analyzed for their FRET efficiency and ROS production (see **Figures S25- S31**). Despite concentration-dependent fluorescence quenching, the most effective combination of Acridine Orange and Rose Bengal was found to be an equivalent ratio. This combination was then investigated for ROS production under 2-PE irradiation using the *in situ* oxidation of $DCFH_2$ (2',7'-dichlorodihydrofluorescein, a non-fluorescent probe) to DCF (2',7'-dichlorofluorescein, a fluorescent one), which is an assay widely used to observe intercellular ROS levels.[51,52] **Figure 4** depicts the time-resolved oxidation of $DCFH_2$ of particles functionalized with the 2-photon absorber Acridine Orange (MOPs-AO (c)), with the photosensitizer Rose Bengal (MOPs-RB (d)), and with both molecules (MOPs-AO-RB (e)). As expected, particles that were only functionalized with either of the dyes resulted in low oxidized DCF. The combination of both functionalizations led to the synergistic enhancement of ROS production (see **Figure 4e** and **Supporting Information** for the corresponding movie). A closer look at the *in-situ* observation of the first few seconds is particularly impressive, as it was possible to see exactly how the ROS is generated in the

immediate vicinity of individual particles or particle agglomerates (see **Figure 4e**). To obtain semi-quantitative results, eight positions of each sample were measured and the mean fluorescence intensity of the DCF channel was plotted against time (see **Figure 4b**), which clearly underlines the message of the fluorescence images. The toxic effect of the produced ROS was also evaluated on cancer cells. While non-irradiated are vital, cells that have been irradiated are no longer viable which could be shown by Calcein AM staining (see **Figures S32** and **S33**).

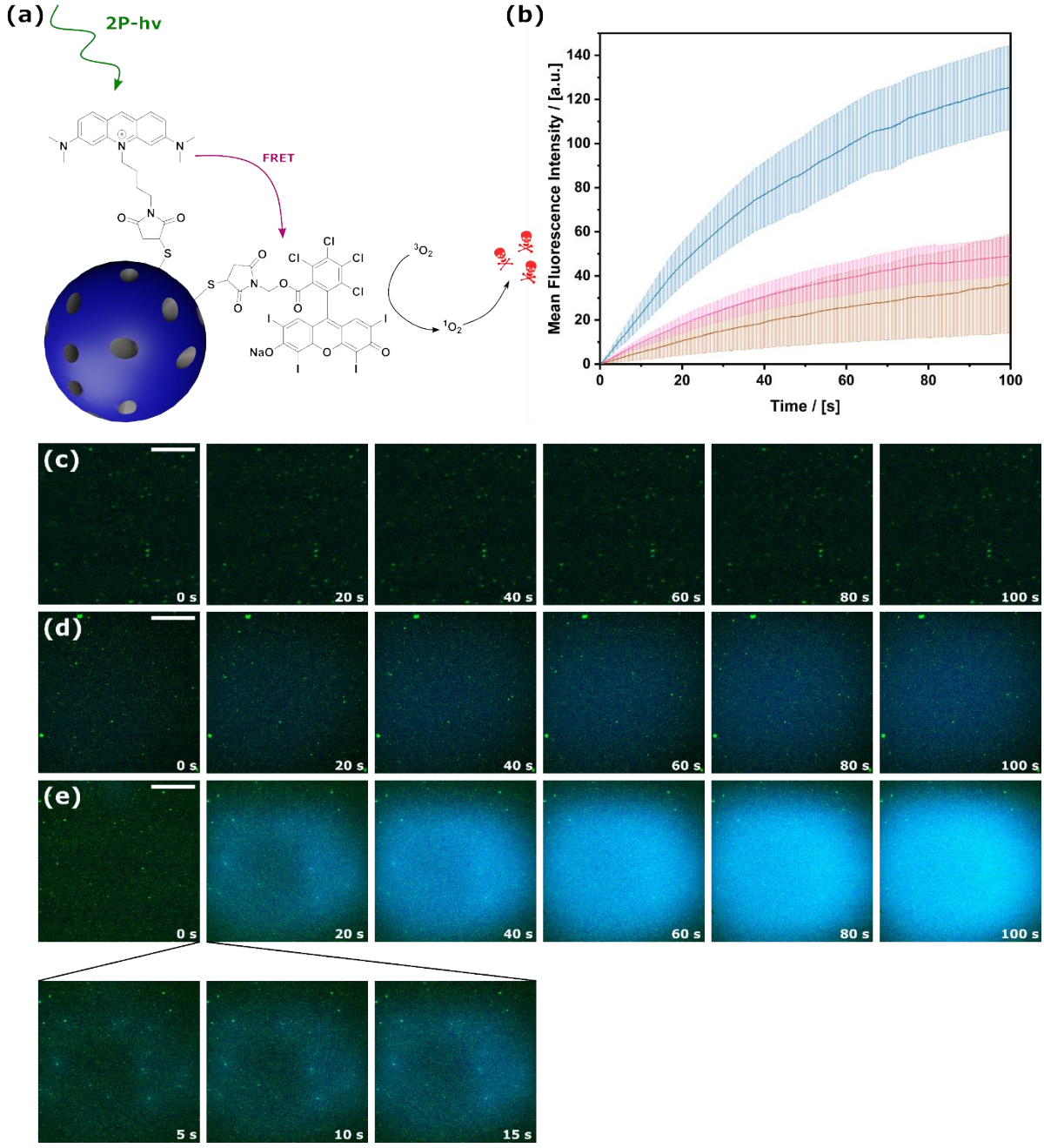

Figure 2: a) Schematic structure of binary MOPs-AO-RB. b) Increasing mean fluorescence intensity that equals the ROS production (monitored by the reaction of non-fluorescent DCFH with ROS and forming fluorescent $DCFH_2$) of MOPs-AO (brown), MOPs-RB (pink) and MOPs-AO-RB (blue) by averaging the fluorescence intensity of 8 individual experiments (error bars show the standard deviation). Exemplary time-resolved ROS production

of MOPs-AO (c), MOPs-RB (d), and combined MOPs-AO-RB (e). Particles are pseudo-colored in green and the DCF signal pseudo-colored in blue. Scale bar corresponds to 50 µm.

2.3 Trifunctional particles combining 2-photon absorption, ROS production, and small molecule release

Finally, the ROS-triggered small molecule release functionalization was combined with 2-photon activation for application in deep tissue in trifunctional particles (see **Scheme 1**). As this advanced system required a straightforward read-out, thymol was replaced by a model drug that can be detected *in situ* by fluorescence. In order not to interfere with the FRET system, the model drug should not absorb in the area of Acridine Orange or Rose Bengal. For this purpose, umbelliferone was selected, which can also be functionalized with the ROS-cleavable linker (as seen in **Scheme S4**). The detailed synthetic procedure can be found in the supporting information. The resulting MOPs-AO-RB-ROSUmb were characterized profoundly regarding the post-functionalization and results can be found in **Figures S35- S43**, which verified the immobilization of all three components. It is noteworthy that the FRET efficiency of the ternary materials decreased to 74%, most probably due to the third functionalization which is not able to absorb energy from the excited Acridine Orange.

The release behavior of MOPs-AO-RB-ROSUmb was first tested under single-photon irradiation in water. The results can be found in **Figure S44**. After an irradiation time of 30 min, 23% of the immobilized umbelliferon was released which is seven times higher than the release in the dark. HPLC and ESI-MS analyses proved its intactness after release (see **Figure S45**). Also, when examining the supernatant for fluorescence properties (see **Figure 5b**), the solution showed an expected fluorescence band at 455 nm when irradiated at 325 nm. This is similar to the fluorescence emission of pure umbelliferon and, thus, additionally verified no impairment of the molecular structure by release and basis for the subsequent *in situ* detection.

After having shown the general suitability of umbelliferon as model released drug, the system was tested with 2-photon excitation. However, when trying to detect the released compound in water, the advantage of the precise resolution of the laser turned into a drawback: The diffusion of the compound was too fast and, thus, no fluorescence could be detected. To circumvent this problem, a higher viscous liquid was chosen for the following experiments. Changing the solvent did neither change the ability of MOPs-AO-RB-ROSUmb to produce $^1O_2$ (see **Figure S46**) nor the release umbelliferone (see **Figure S48**), both could be verified by conducting the corresponding assays in the different solvent. To ensure that the release in glycerol was still based on the mechanism of ROS-induced cleavage of the linker, the release in the dark was

analyzed as well. Changing the solvent from water to glycerol did not have a negative influence on the stability of the linker (see **Figures S48- S50**). Thus, the modified system and experimental setup fulfilled all requirements to detect the release of a fluorescent drug upon irradiation with 2-photon excitation. **Figure 5c** depicts the result of the 2-photon excitation of MOPs-AO-RB-ROSUmb. The particles themselves could be detected due to their fluorescence. When the particles were irradiated, the release of umbelliferone could be detected *in situ*, as a second emission can be detected around the particles which can be attributed to the free umbelliferone (see also **movie in Supporting Information**). To the best of our knowledge, this is the first time that the release of an antibacterial drug was detected *in situ* upon the ROS-triggered cleavage of an oxidative sensitive linker with 2-photon irradiation.

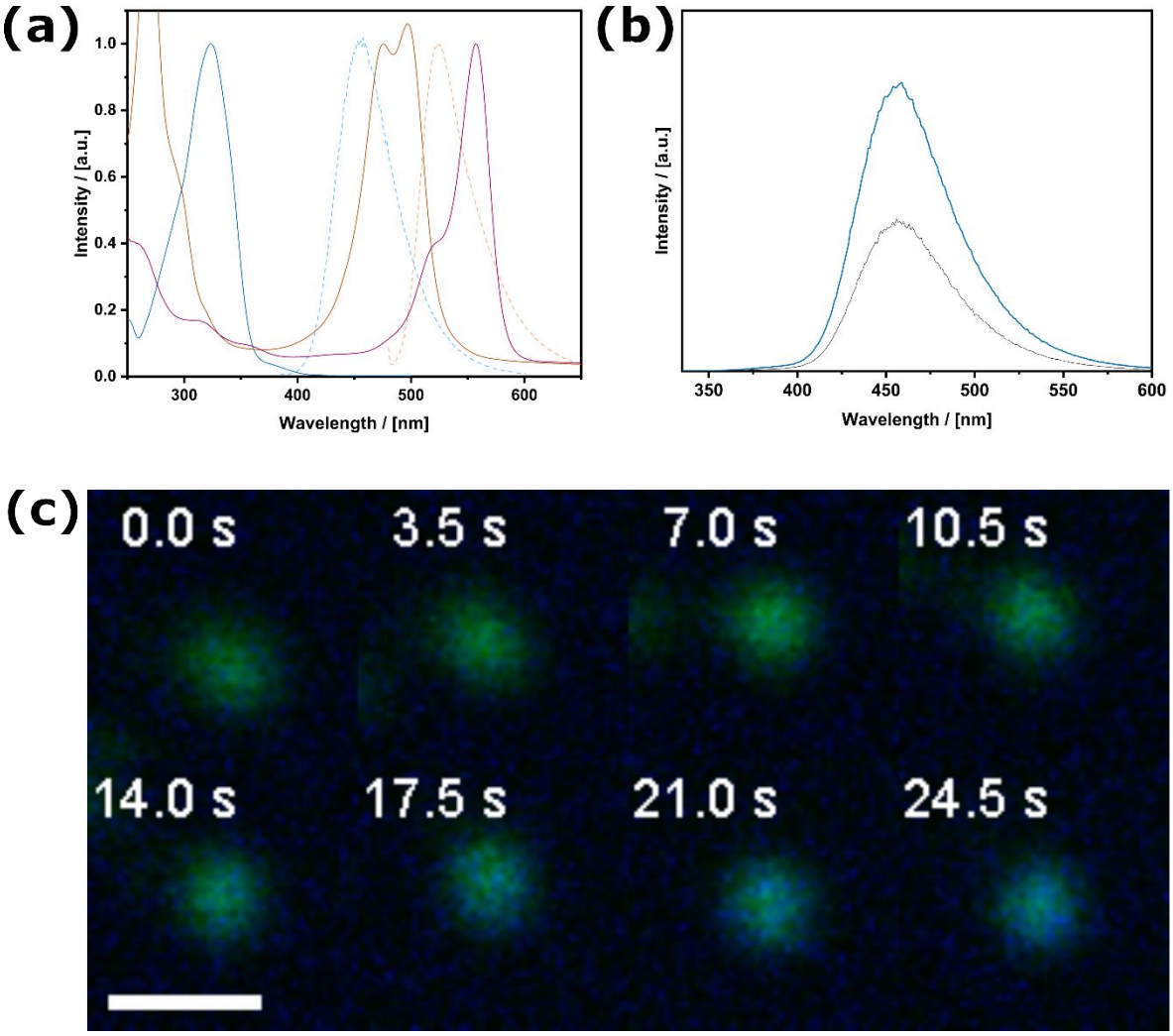

Figure 3: a) Absorption and emission of umbelliferone (absorption in dark blue, emission in dotted blue), Mal-Acridine Orange (absorption in brown, emission in dotted brown), Mal-Rose Bengal (absorption in pink). b) Fluorescence emission of released umbelliferone from MOPs-AO-RB-ROSUmb (blue) compared to umbelliferone (grey). c) In-situ detection of released umbelliferone (blue) from MOPs-AO-RB-ROSUmb (pseudo-colored in green) under 2-PE irradiation. Scale bar corresponds to 500 nm.

3. Conclusion

In the presented work, we reported the synthesis of multifunctional MOPs and their potential as light-triggered biocidal materials. For this purpose, MOPs that possess a high density of thiol groups on their surface were used, allowing for immobilization of more than one antibacterial function onto one particle by thiol-maleimide click chemistry. By covalently binding the photosensitizer Rose Bengal onto the material, the material is capable of producing reactive oxygen species upon light irradiation. Due to the short diffusion range of reactive oxygen species, one aim of this study was to add another antibacterial function to the material to increase its range of activity. By this, the light irradiation was intended to initiate a cascade reaction first generating ROS, which can then cleave a linker to release an antibacterial agent. As there is a strong need for alternatives to antibiotics, we focused on the release of the essential oil thymol which is a known anti-quorum sensing inhibitor and a novel strategy to overcome the problem of infections by resistant pathogens. Initial antibacterial tests showed promising results regarding the biocidal effect of thymol. Nevertheless, these results will be further investigated and the materials tested for their optimal antibacterial behavior.

To solve the demanding task of the low penetration depth of the light into the tissue, we further focused on the use of light in the therapeutic window (with a range of 650 to 1350 nm), as this is the range in which the light has the maximum penetration depth. Therefore, we used the effect of two-photon excitation, i.e. the simultaneous absorption of two photons with only half the frequency, to transfer a molecule from the ground state to its excited state instead of using a photon with twice the frequency. Thereby, we immobilized two dyes with corresponding optical properties and used the FRET of Acridine Orange that absorbs light generated by 2-PE irradiation and transfers it onto Rose Bengal which is a photosensitizer. We were able to demonstrate the increased ROS production of the binary particles in *in situ* measurements. In a last and sophisticated experiment, we united the knowledge that we have gained in the first and second part of the work and generated trifunctional particles that are functionalized with the FRET pair and an additional third fluorescent small molecule that can also be exemplary for any antibacterial drug. Under irradiation with 2-PE, we could monitor the *in situ* release of the fluorescent dye. These first results of the model system open the door for further interesting material developments in the context of anti-bacterial implant coatings as they could be triggered by and treat implant-associated infections in a non-invasive manner without removal of the complete implant. A future destination would be a material that combines the therapeutic effect with a sensor that indicates the presence of a bacterial infection. A material designed in

this way could have a major impact and mean that surgical methods are no longer required for the treatment of bacterial implant infections.

4. Experimental Section/Methods

Experimental Details can be found in the Supporting Information.

Supporting Information

Supporting Information is available from the author.

Acknowledgements

References

[1] C. J. L. Murray, K. S. Ikuta, F. Sharara, L. Swetschinski, G. R. Aguilar, A. Gray, C. Han, C. Bisignano, P. Rao, E. Wool, S. C. Johnson, A. J. Browne, M. G. Chipeta, F. Fell, S. Hackett, G. Haines-Woodhouse, B. H. K. Hamadani, E. A. P. Kumaran, B. McManigal, S. Achalapong, R. Agarwal, S. Akech, S. Albertson, J. Amuasi, J. Andrews, A. Aravkin, E. Ashley, F.-X. Babin, F. Bailey, S. Baker, B. Basnyat, A. Bekker, R. Bender, J. A. Berkley, A. Bethou, J. Bielicki, S. Boonkasidecha, J. Bukosia, C. Carvalheiro, C. Castañeda-Orjuela, V. Chansamouth, S. Chaurasia, S. Chiurchiù, F. Chowdhury, R. C. Donatien, A. J. Cook, B. Cooper, T. R. Cressey, E. Criollo-Mora, M. Cunningham, S. Darboe, N. P. J. Day, M. D. Luca, K. Dokova, A. Dramowski, S. J. Dunachie, T. D. Bich, T. Eckmanns, D. Eibach, A. Emami, N. Feasey, N. Fisher-Pearson, K. Forrest, C. Garcia, D. Garrett, P. Gastmeier, A. Z. Giref, R. C. Greer, V. Gupta, S. Haller, A. Haselbeck, S. I. Hay, M. Holm, S. Hopkins, Y. Hsia, K. C. Iregbu, J. Jacobs, D. Jarovsky, F. Javanmardi, A. W. J. Jenney, M. Khorana, S. Khusuwan, N. Kissoon, E. Kobeissi, T. Kostyanev, F. Krapp, R. Krumkamp, A. Kumar, H. H. Kyu, C. Lim, K. Lim, D. Limmathurotsakul, M. J. Loftus, M. Lunn, J. Ma, A. Manoharan, F. Marks, J. May, M. Mayxay, N. Mturi, T. Munera-Huertas, P. Musicha, L. A. Musila, M. M. Mussi-Pinhata, R. N. Naidu, T. Nakamura, R. Nanavati, S. Nangia, P. Newton, C. Ngoun, A. Novotney, D. Nwakanma, C. W. Obiero, T. J. Ochoa, A. Olivas-Martinez, P. Olliaro, E. Ooko, E. Ortiz-Brizuela, P. Ounchanum, G. D. Pak, J. L. Paredes, A. Y. Peleg, C. Perrone, T. Phe, K. Phommasone, N. Plakkal, A. Ponce-de-Leon, M. Raad, T. Ramdin, S. Rattanavong, A. Riddell, T. Roberts, J. V. Robotham, A. Roca, V. D. Rosenthal, K. E. Rudd, N. Russell, H. S. Sader, W. Saengchan, J. Schnall, J. A. G. Scott, S. Seekaew, M. Sharland, M. Shivamallappa, J. Sifuentes-Osornio, A. J. Simpson, N. Steenkeste, A. J. Stewardson, T. Stoeva, N. Tasak, A. Thaiprakong, G. Thwaites, C. Tigoi, C. Turner, P. Turner, H. R. van Doorn, S. Velaphi, A. Vongpradith, M. Vongsouvath, H. Vu, T. Walsh, J. L. Walson, S. Waner, T. Wangrangsimakul, P. Wannapinij, T. Wozniak, T. E. M. W. Y. Sharma, K. C. Yu, P. Zheng, B. Sartorius, A. D. Lopez, A. Stergachis, C. Moore, C. Dolecek, M. Naghavi, *The Lancet* **2022**, *399*, 629–655.

[2] "2021 antibacterial agents in clinical and preclinical development: an overview and analysis," can be found under https://www.who.int/publications-detail-redirect/9789240047655, **n.d.**

[3] R. Zhang, M. Hua, H. Liu, J. Li, *MATERIALS SCIENCE AND ENGINEERING B-ADVANCED FUNCTIONAL SOLID-STATE MATERIALS* **2021**, *263*, 114835.

[4] J. Parra-Nieto, M. A. G. del Cid, I. A. de Carcer, A. Baeza, *BIOTECHNOLOGY*

JOURNAL **2021**, *16*, 2000150.
[5] T. A. Esquivel-Castro, M. C. Ibarra-Alonso, J. Oliva, A. Martinez-Luevanos, *MATERIALS SCIENCE AND ENGINEERING C-MATERIALS FOR BIOLOGICAL APPLICATIONS* **2019**, *96*, 915–940.
[6] Y. Liu, R. Qin, S. A. J. Zaat, E. Breukink, M. Heger, *J Clin Transl Res* **2015**, *1*, 140–167.
[7] J. Gehring, B. Trepka, N. Klinkenberg, H. Bronner, D. Schleheck, S. Polarz, *J. Am. Chem. Soc.* **2016**, *138*, 3076–3084.
[8] C. G. Dariva, J. F. J. Coelho, A. C. Serra, *Journal of Controlled Release* **2019**, *294*, 337–354.
[9] H. Bronner, F. Brunswig, D. Pluta, Y. Krysiak, N. Bigall, O. Plettenburg, S. Polarz, *ACS Appl. Mater. Interfaces* **2023**, *15*, 14067–14076.
[10] S. Wu, H.-J. Butt, *Advanced Materials* **2016**, *28*, 1208–1226.
[11] S.-H. Cheng, C.-C. Hsieh, N.-T. Chen, C.-H. Chu, C.-M. Huang, P.-T. Chou, F.-G. Tseng, C.-S. Yang, C.-Y. Mou, L.-W. Lo, *Nano Today* **2011**, *6*, 552–563.
[12] H. Liu, Y. Yang, A. Wang, M. Han, W. Cui, J. Li, *Advanced Functional Materials* **2016**, *26*, 2561–2570.
[13] Sytsma, Vroom, D. Grauw, Gerritsen, *Journal of Microscopy* **1998**, *191*, 39–51.
[14] T. R. Neu, U. Kuhlicke, J. R. Lawrence, *Applied and Environmental Microbiology* **2002**, DOI 10.1128/AEM.68.2.901-909.2002.
[15] F. Bestvater, E. Spiess, G. Stobrawa, M. Hacker, T. Feurer, T. Porwol, U. Berchner-Pfannschmidt, C. Wotzlaw, H. Acker, *Journal of Microscopy* **2002**, *208*, 108–115.
[16] K. A. Hammer, C. F. Carson, T. V. Riley, *Journal of Applied Microbiology* **1999**, *86*, 985–990.
[17] M. Cáceres, W. Hidalgo, E. Stashenko, R. Torres, C. Ortiz, *Antibiotics* **2020**, *9*, 147.
[18] K. Kachur, Z. Suntres, *Critical Reviews in Food Science and Nutrition* **2020**, *60*, 3042–3053.
[19] N. Høiby, T. Bjarnsholt, M. Givskov, S. Molin, O. Ciofu, *International Journal of Antimicrobial Agents* **2010**, *35*, 322–332.
[20] C. Wang, J. Hou, H. C. van der Mei, H. J. Busscher, Y. Ren, *mBio* **2019**, *10*, e01908-19.
[21] E. Paluch, J. Rewak-Soroczyńska, I. Jędrusik, E. Mazurkiewicz, K. Jermakow, *Appl Microbiol Biotechnol* **2020**, *104*, 1871–1881.
[22] M. Hyldgaard, T. Mygind, R. Meyer, *Frontiers in Microbiology* **2012**, *3*.
[23] A. Nostro, A. S. Roccaro, G. Bisignano, A. Marino, M. A. Cannatelli, F. C. Pizzimenti, P. L. Cioni, F. Procopio, A. R. Blanco, *Journal of Medical Microbiology* **2007**, *56*, 519–523.
[24] J. Dong, L. Zhang, Y. Liu, N. Xu, S. Zhou, Q. Yang, Y. Yang, X. Ai, *Microorganisms* **2020**, *8*, 636.
[25] D. James Bound, P. S. Murthy, P. S. Negi, P. Srinivas, *LWT* **2020**, *122*, 108987.
[26] Y. Zhang, J. Kong, Y. Xie, Y. Guo, Y. Cheng, H. Qian, W. Yao, *LWT* **2018**, *92*, 133–139.
[27] S. Alibi, W. Ben Selma, J. Ramos-Vivas, M. A. Smach, R. Touati, J. Boukadida, J. Navas, H. Ben Mansour, *Current Research in Translational Medicine* **2020**, *68*, 59–66.
[28] A. Sharifi, A. Mohammadzadeh, T. Zahraei Salehi, P. Mahmoodi, *Journal of Applied Microbiology* **2018**, *124*, 379–388.
[29] M. J. Darre, A. Kollanoor-Johny, K. Venkitanarayanan, I. Upadhyaya, *Journal of Applied Poultry Research* **2014**, *23*, 340–344.
[30] C. Piombino, H. Lange, F. Sabuzi, P. Galloni, V. Conte, C. Crestini, *Molecules* **2020**, *25*, 866.
[31] S. Milovanovic, D. Markovic, K. Aksentijevic, D. B. Stojanovic, J. Ivanovic, I.

Zizovic, *Carbohydrate Polymers* **2016**, *147*, 344–353.
[32] M. Mastromatteo, G. Barbuzzi, A. Conte, M. A. Del Nobile, *Innovative Food Science & Emerging Technologies* **2009**, *10*, 222–227.
[33] C. Piombino, H. Lange, F. Sabuzi, P. Galloni, V. Conte, C. Crestini, *Molecules* **2020**, *25*, 866.
[34] M. Fatima, W. H. Almalki, T. Khan, A. Sahebkar, P. Kesharwani, *ADVANCED MATERIALS* **2024**, DOI 10.1002/adma.202312939.
[35] X. Hu, H. Zhang, Y. Wang, B.-C. Shiu, J.-H. Lin, S. Zhang, C.-W. Lou, T.-T. Li, *Chemical Engineering Journal* **2022**, *450*, 138129.
[36] C. G. Dariva, J. F. J. Coelho, A. C. Serra, *Journal of Controlled Release* **2019**, *294*, 337–354.
[37] J. Li, Z. Ding, Y. Li, J. Miao, W. Wang, K. Nundlall, S. Chen, *Materials & Design* **2020**, *195*, 109021.
[38] J. Gehring, D. Schleheck, B. Trepka, S. Polarz, *ACS APPLIED MATERIALS & INTERFACES* **2015**, *7*, 1021–1029.
[39] T. Entradas, S. Waldron, M. Volk, *Journal of Photochemistry and Photobiology B: Biology* **2020**, *204*, 111787.
[40] A. Sharma, M.-G. Lee, M. Won, S. Koo, J. F. Arambula, J. L. Sessler, S.-G. Chi, J. S. Kim, *J. Am. Chem. Soc.* **2019**, *141*, 15611–15618.
[41] J. Ostergaard, C. Larsen, *Molecules* **2007**, *12*, 2396–2412.
[42] M. Imran, A. Rauf, I. A. Khan, M. Shahbaz, T. B. Qaisrani, S. Fatmawati, T. Abu-Izneid, A. Imran, K. U. Rahman, T. A. Gondal, *Biomedicine & Pharmacotherapy* **2018**, *106*, 390–402.
[43] P. Tantivitayakul, R. Kaypetch, T. Muadchiengka, *Archives of Oral Biology* **2020**, *115*, 104744.
[44] K. Chaieb, B. Kouidhi, H. Jrah, K. Mahdouani, A. Bakhrouf, *BMC Complementary and Alternative Medicine* **2011**, *11*, 29.
[45] A. A. Dera, I. Ahmad, P. Rajagopalan, M. A. Shahrani, A. Saif, M. Y. Alshahrani, Y. Alraey, A. M. Alamri, S. Alasmari, M. Makkawi, A. G. Alkhathami, G. Zaman, A. Hakami, R. Alhefzi, M. A. Alfhili, *Saudi Med J* **2021**, *42*, 196–204.
[46] R. Mishra, A. K. Panda, S. De Mandal, M. Shakeel, S. S. Bisht, J. Khan, *Frontiers in Microbiology* **2020**, *11*, 2640.
[47] M. Lu, Y. Li, M. X. Wu, *Commun Biol* **2021**, *4*, 1–12.
[48] K. Doll, K. L. Jongsthaphongpun, N. S. Stumpp, A. Winkel, M. Stiesch, *Journal of Microbiological Methods* **2016**, *130*, 61–68.
[49] J. Gehring, B. Trepka, N. Klinkenberg, H. Bronner, D. Schleheck, S. Polarz, *J. Am. Chem. Soc.* **2016**, *138*, 3076–3084.
[50] N. Heine, K. Doll-Nikutta, F. Stein, J. Jakobi, A. Ingendoh-Tsakmakidis, C. Rehbock, A. Winkel, S. Barcikowski, M. Stiesch, *Sci Rep* **2024**, *14*, 3405.
[51] J. James, N. Fiji, D. Roy, D. A. Mg, M. Sham Shihabudeen, D. Chattopadhyay, K. Thirumurugan, *Analytical Methods* **2015**, *7*, 8572–8575.
[52] E. Eruslanov, S. Kusmartsev, in *Advanced Protocols in Oxidative Stress II* (Ed.: D. Armstrong), Humana Press, Totowa, NJ, **2010**, pp. 57–72.